Validation of a Turbulent Kelvin-Helmholtz Shear Layer Model Using a High-Energy-Density OMEGA Laser Experiment

O. A. Hurricane, V. A. Smalyuk, K. Raman, O. Schilling, J. F. Hansen, G. Langstaff, D. Martinez, H.-S. Park, B. A. Remington, H. F. Robey, J. A. Greenough, R. Wallace, C. A. Di Stefano, R. P. Drake, D. Marion, C. M. Krauland, and C. C. Kuranz

Validation of a Turbulent Kelvin–Helmholtz Shear Layer Model using a High Energy Density OMEGA Laser Experiment
LLNL-JRNL-553731-DRAFT, 2012

O. A. Hurricane, V. A. Smalyuk, K. Raman, O. Schilling, J. F. Hansen, G. Langstaff, D. Martinez, H.-S. Park, B. A. Remington, H. F. Robey, J. A. Greenough, and R. Wallace

Lawrence Livermore National Laboratory
*P.O. Box 808, Livermore, California 94551**

C. A. Di Stefano, R. P. Drake, D. Marion, C. M. Krauland, and C. C. Kuranz

Department of Atmospheric, Oceanic, and Space Sciences,
University of Michigan, Ann Arbor, Michigan 48109

Following the successful demonstration of an OMEGA laser-driven platform for generating and studying nearly two-dimensional unstable plasma shear layers [Hurricane et al., Phys. Plasmas **16** 056305 (2009); Harding et al., Phys. Rev. Lett., **103** 045005 (2009)], this Letter reports on the first quantitative measurements of turbulent mixing in a high energy density plasma. As a blast-wave moves parallel to an unperturbed interface between a low density foam and a high density plastic, baroclinic vorticity is deposited at the interface and a Kelvin–Helmholtz instability-driven turbulent mixing layer is created in the post-shock flow due to surface roughness. The spatial scale and density profile of the turbulent layer are diagnosed using x-ray radiography with sufficiently small uncertainty that the data can be used to constrain turbulent mixing models. The estimated Reynolds number ($\sim 10^6$), Liepmann–Taylor scale ($\sim 0.5~\mu$m) and inner viscous scale ($\sim 0.17~\mu$m) in the post-shock plasma flow are consistent with an "inertial subrange" within which a Kolmogorov turbulent energy cascade can be active. An illustration of comparing the data set with the predictions of a two-equation turbulence model in the ARES radiation hydrodynamics code is also presented.

PACS numbers: 47.20.Ft, 47.27.wj, 52.35.Ra, 52.35.Tc, 52.57.Fg

Kelvin–Helmholtz (KH) instability arising from shear flow is key to many hydrodynamic mixing processes. In high energy density plasma (HEDP) contexts, Kelvin–Helmholtz instability is important in inertial confinement fusion (ICF) and astrophysical mixing, usually as a consequence of acceleration-driven Rayleigh–Taylor (RT) instability or shock-driven Richtmyer–Meshkov (RM) instability, but also as a primary instability such as in molecular cloud structure [1]. In the context of ICF, even small amounts of mixing can have large effects on the energy released by fusion. While unstable shear layers in fluids have been studied for decades, e.g. [2–5], only recently has an HEDP analog of these classical shear layers been created [6, 7] using targets with a pre-imposed sinusoidal interfacial perturbation fielded on the OMEGA laser facility at the University of Rochester Laboratory for Laser Energetics [8]. In this Letter, we present results of an experiment designed to produce an HEDP turbulent shear layer growing in a target configuration with no pre-imposed perturbation (other than surface finish), together with a comparison of these data with a simulation using a two-equation Reynolds-averaged turbulence model. The turbulence model and the best-fit coefficients for this experiment are briefly described.

The basic configuration (see Fig. 1) consists of a 400 μm polyamide-imide ($C_{22}H_{14}O_4N_2$, $\rho = 1.40$ g/cm^3) plastic laminated on each side of a 200 μm thick iodinated polystyrene (CHI; $C_{50}H_{47}I_3$, $\rho = 1.43$ g/cm^3) opaque layer stacked under a carbon resorcinol foam ($C_{1000}O_{45}H_{65}$, $\rho = 0.1$ g/cm^3). This package is contained within a beryllium (Be) shock tube of rectangular cross-section, so as to be able to radiograph through it with x-rays from the 5.18 keV He-α transition of laser-heated vanadium backlighter foil. The lamination of plastic and the carbon foam are each 1 mm square cross-section parts that are 4 mm long. The Be tube walls are 0.2 mm thick on the vertical sides and 0.5 mm thick on the top and bottom. The surface roughness of the plastic 'sandwich' part ranges from 50–100 nm with a flat Fourier spectrum. Laser energy (~ 4.3 kJ in a 1 ns pulse) is delivered to an 820 μm diameter (full-width half-maximum) super-Gaussian profile ($N = 4.7$) spot on a C_8H_8 ablator ($\rho = 1.05$ g/cm^3) covering the low density foam part of the target. A strong shock is launched into the low density foam such that the pressure gradient at the leading edge of the shock is at right angles to the density gradient through the interface separating the two dissimilar materials, thus maximizing the baroclinic vorticity production proportional to $\nabla p \times \nabla \rho$ [10]. Once the laser is fired at the target, the ensuing flow evolves for tens of nanoseconds before an image of the target and instability development are captured onto D-8 x-ray film using point projection backlighting. The field of view of the image taken is approximately 2 mm in diameter. Further details of the target design can be found in [6, 10] while further details on the most recent experimental configuration and
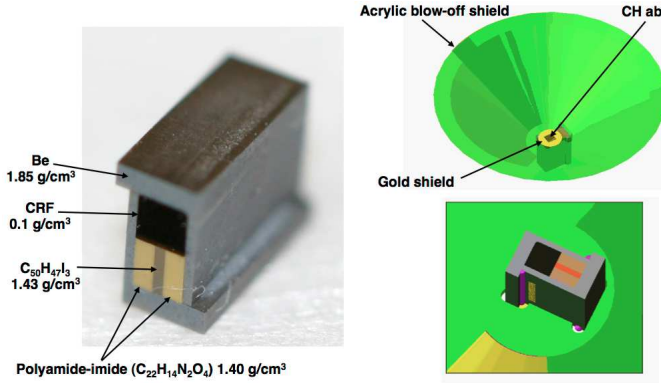
FIG. 1: (color online.) A photograph of the 4 mm long target (left) before being combined with the plasma shielding (right). Materials are labeled in the figure. The laser energy is imparted on the carbon resorcinol foam (CRF) surface shown, and is incident on a 30 μm thick plastic ablator that covers this end of the target.
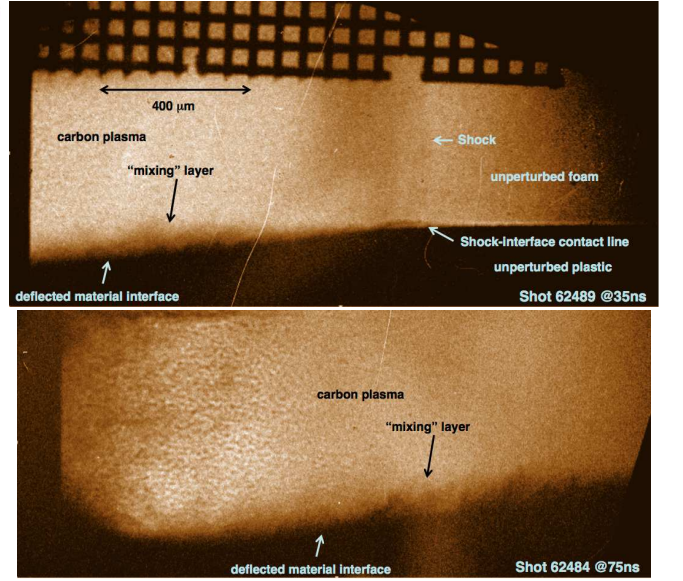

FIG. 2: (color online.) Radiographs from two shots at $t = 35$ ns (top) and $t = 75$ ns (bottom) showing the development of a shear mixing layer at the interface between the iodinated plastic (the dark opaque material in the lower part of each image) and the foam (the lighter region). In the $t = 35$ ns image, the incident shock and fiducial grid are also seen. The shock wave is moving from left to right.

a discussion of the full suite of target configurations and resulting data can be found elsewhere [9].

Data images of shot 62489 and shot 62484 show the hydrodynamics of the target package at $t = 35$ and $t = 75$ ns, respectively (Fig. 2). The image resolution is 17 μm. The upper image at $t = 35$ ns shows a smooth contact boundary between the unshocked foam and unshocked plastic on the right-hand side, the rightward traveling shock just to the right of center, and the mixing layer in the post-shock flow on the left-hand side. The mixing layer is seen to be expanding spatially in the y-direction as a function of distance from 0–900 μm behind the shock. The second image taken at $t = 75$ ns shows an even wider mixing layer at the same x-location on the target. The modulations above the layer at late time are the manifestation of an instability resulting from the three-dimensional expansion of the foam–Be interface in the foreground/background that are being radiographed [19]. The numerical simulations discussed below show that, at $x = 0.15$ cm the center of the field of view of the data, immediately after the passage of the ~ 2 Mbar blast-wave [with shock position, $X_s \sim (E/\rho)^{1/3} t^{2/3}$, scaling as the classical one-dimensional self-similar Taylor-like solution] the post-shock flow speed spikes to ~ 45 μm/ns and decays to zero at a distance ~ 1300 μm behind the shock, thus limiting the extent of the most rapid growth of shear mixing to a region immediately behind the shock. The radiation temperature in the post-shock flow is ~ 9 eV and is expected to be in equilibrium with the material. The maximum visible (corresponding to a density of 0.01 g/cm^3) extent of the mixing layer of CHI into the foam is measured to be ~ 100 μm.

Evidence indicates that turbulent mixing develops [14–16] when the Liepmann–Taylor scale ($\lambda_{LT} \approx 5\zeta Re^{-1/2}$) exceeds the inner-viscous scale ($\lambda_\nu \approx 50\zeta Re^{-3/4}$). These

are estimated as 0.5 μm and 0.17 μm, respectively (based on a viscosity $\nu \sim 0.014$ cm^2/s and Reynolds number $\sim 10^6$, both inferred from the data [7] using the estimates in [12], and an outer flow scale $\zeta \sim 100$ μm). The difference between these scales corresponds to the "inertial subrange" within which the Kolmogorov turbulent energy cascade can be active. Above the Liepmann–Taylor scale, imposed forcing scales of the flow dominate, while below the inner-viscous scale viscous damping dominates. The viscous diffusion scale $\sqrt{\nu t} \sim 0.037$ μm is very much less than the observed ~ 100 μm scale, indicating that molecular diffusion is not responsible for the observed layer growth. While turbulent shear layers have been suspected to exist in previous HED and ICF experiments, the present experiment is the first to intentionally create and diagnose such a feature. Obtaining such data is essential for calibrating turbulence models that are applied to a variety of HEDP and ICF flows.

We discuss turbulent mix modeling within the conceptual framework described by Dimonte and Tipton (DT) [20] and references therein. The model is based on a Reynolds decomposition of the fluid equations, supplemented by equations for the specific turbulent energy density, K, and the scale of the turbulence, L (in effect the largest eddy size). This yields a closed set of equations in which there are several coefficients that represent physically the correlations of the fluctuations in the fluid. One can reasonably hope that the correlation coefficients will have similar values over a substantial range

of fluid conditions. This "K-L" turbulent mixing model is implemented in the multidimensional radiation hydrodynamics code ARES [17, 18] developed at the Lawrence Livermore National Laboratory. The model includes a shock-compatible treatment of the off-diagonal terms in the stress tensor, needed to model unstable shear flows. The mean flow equations solved are

$$\rho \frac{du_i}{dt} = -\frac{\partial}{\partial x_i}(p + p_t) + \frac{\partial \tau_{ij}}{\partial x_j}, \quad (1)$$

$$\rho \frac{dU}{dt} = b_t \frac{L\sqrt{K}}{\rho} \frac{\partial \rho}{\partial x_j} \frac{\partial p}{\partial x_j} - p \frac{\partial u_j}{\partial x_j} \quad (2)$$
$$+ d_t \frac{\rho K^{3/2}}{L} + \frac{\partial}{\partial x_j}\left(\frac{\mu_t}{Pr_t} \frac{\partial U}{\partial x_j}\right),$$

$$\rho \frac{dm_r}{dt} = \frac{\partial}{\partial x_j}\left(\frac{\mu_t}{Sc_t} \frac{\partial m_r}{\partial x_j}\right), \quad (3)$$

where $d/dt = \partial/\partial t + u_j \partial/\partial x_j$ is the Lagrangian derivative, ρ is the mean density, u_i is the mean velocity, p is the mean pressure, U is the mean specific internal energy, m_r are the mean species mass fractions (r denotes the species), $\mu_t = a_t \rho L \sqrt{K}$ is the turbulent dynamic viscosity, and $p_t = (2/3)\rho K$ is the turbulent pressure. The relation of the stress tensor to the strain rate is $\tau_{ij} = -2 v_s \mu_t S_{ij}$ with mean strain-rate tensor $S_{ij} = \frac{1}{2}\left(\frac{\partial u_i}{\partial x_j} + \frac{\partial u_j}{\partial x_i}\right) - \frac{1}{3}\frac{\partial u_k}{\partial x_k}\delta_{ij}$, where δ_{ij} is the Kronecker delta. The turbulence equations are

$$\rho \frac{dK}{dt} = -b_t \frac{L\sqrt{K}}{\rho} \frac{\partial \rho}{\partial x_j} \frac{\partial p}{\partial x_j} - p_t \frac{\partial u_j}{\partial x_j} - \tau_{ij} S_{ij} \quad (4)$$
$$- d_t \frac{\rho K^{3/2}}{L} + \frac{\partial}{\partial x_j}\left(\frac{\mu_t}{\sigma_K} \frac{\partial K}{\partial x_j}\right),$$

$$\rho \frac{dL}{dt} = l_{1t} \rho L \frac{\partial u_j}{\partial x_j} + l_{2t} \rho \sqrt{2K} + \frac{\partial}{\partial x_j}\left(\frac{\mu_t}{\sigma_L} \frac{\partial L}{\partial x_j}\right). \quad (5)$$

The molecular viscosity, diffusivity and conductivity are assumed to be negligible in this model compared to the turbulent diffusion terms [the last terms in Eqs. (2)–(5)]. The shear production of turbulence in the model is largely due to the $-\tau_{ij}S_{ij}$ term.

The correlation coefficients in this model are not truly independent. Based on the sensible expectation that the turbulent evolution should be self-similar, DT find that one should take $\sigma_L = \sigma_K = Pr_t = Sc_t = 1.0$. We follow DT in taking $a_t = \sqrt{2}$ (for our definitions), which models well the non-KH experiments they consider. This leaves the adjustment in the stress tensor needed to model KH systems to the parameter v_s. Of the three remaining parameters in the model, the two related to compressible effects (ℓ_{1t} and b_t) and the one related to viscous dissipation (d_t) all have small effects in this high-Reynolds-number, mostly subsonic flow. These are set, based on modeling of other hydrodynamic instability experiments
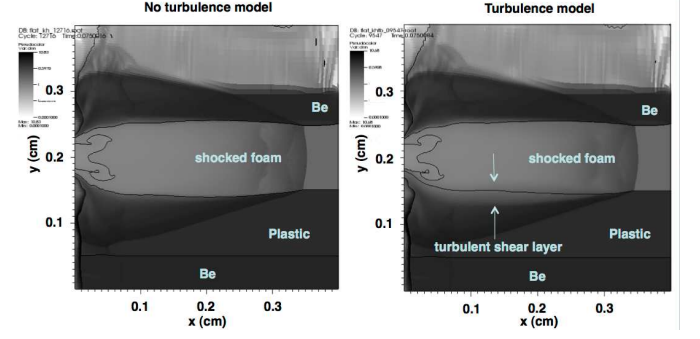

FIG. 3: ARES results are shown for simulations of the experiment with no turbulence model (left) and with the K-L turbulence model with the coefficients described in the text (right). The simulation without turbulence shows a distinct discontinuity in density at the foam plastic interface, while the simulation with the turbulence model diffuses the two materials around the "interface" (thin black contours) defined by a 50% mass fraction. The mixing layer width is denoted in the figure by the opposing arrows. The shock, traveling from left to right, is seen in the foam at a position slightly beyond $x = 0.3$ cm at $t = 75$ ns.

[20], to $b_t = 1.2, d_t = 3.5$, and $\ell_{1t} = 0.8$. The parameter ℓ_{2t}, multiplying the term by which the turbulence drives growth of the eddies, is taken to be 1.0 following DT, who point out that as yet there is no experimental grounds for any other value.

The leading behavior for a KH turbulent mix layer can be seen by applying the self-similar analysis of DT to KH mixing in an incompressible fluid in which the only spatial variation is provided by the shear flow. Using a self-similar mixing-layer width $h(t) = \delta \Delta v t$, where Δv is the velocity difference of the two streams, one finds $\delta = \sqrt{2} l_{2t} \sqrt{v_s a_t / (l_{2t} + 2)}$. This gives $\delta \approx 0.22$ using $\ell_{2t} = 1, a_t = \sqrt{2}$, and $v_s = 0.05$ (see below). The value of δ is slightly larger than the experimental value $\delta \approx 0.18$ measured in fluid shear layer experiments [22].

The two-dimensional ARES simulation results, using the model above, show the expected hydrodynamic behavior with and without turbulence modeling (see Fig. 3). The simulation includes tabulated material equations of state, tabulated opacities, ionization (based on the Thomas-Fermi model), electron heat conduction, and radiation diffusion. A separate laser energy deposition model described in [6] is used to create an internal energy source per unit mass in the ablator material that drives the hydrodynamics. The spatial resolution used in these simulations is ~ 7 μm (corresponding to a numerical Reynolds number of ~ 600, implying the need for a subgrid turbulence mix model).

Given the opacity of the CHI at the vanadium backlighter energy and thickness of the tracer layer in the experiment, optical depth information contained in the radiographs can be translated into density information that can be compared to simulation. Figure 4 shows pro-
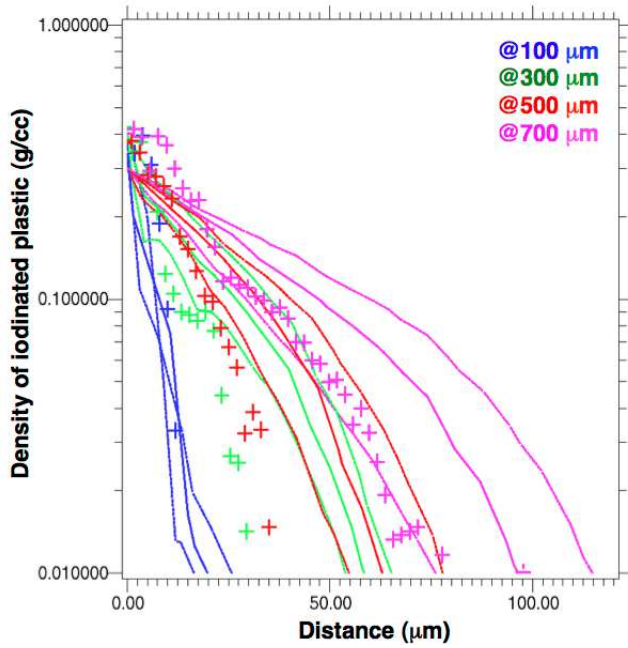
FIG. 4: (color online.) Results of simulation (colored curves) and experiment (crosses), showing at $t = 35$ ns transverse profiles of CHI density at four different axial distances from the shock front (100–700 μm). For each axial location simulation curves are shown for $v_s = 0.05$, 1.0, and 2.0. The experimental uncertainty is ± 0.01 g/cm^3. Densities > 0.5 g/cm^3 cannot be measured because the iodinated plastic has become completely opaque at the backlighter energy used.

files of density along the transverse direction across the observed shear layer, taken at several locations in the post-shock flow generated by the passage of the primary laser-driven shock wave. One can see in the figure that the best overall fit to the profiles at relatively high density, among the values used, is $v_s = 0.05$, which produces profiles reasonably close to those in the data. Examining the leading edge of the mix layer at a lower density of CHI (10^{-4} g/cc), one finds the simulated location to increase from 22 μm ahead of the data to 34 μm ahead of it as v_s is doubled then quadrupled respectively.

The present experiment demonstrates an intentionally produced HED plasma shear layer that is both *turbulent* and *diagnosable*. Notably, we measured the material density gradients in the shear mixing layer in addition to the mixing layer width. It was demonstrated that this data can be used to constrain a K-L turbulence model, which can then be applied to other HED/ICF experiments as well as to astrophysical and other fluid systems. Other turbulence models can similarly be tested against this data. It is desirable to field a larger scale version of this experiment on a higher energy facility such as the National Ignition Facility (NIF) at Lawrence Livermore National Laboratory, as it would allow direct observation of the Liepmann–Taylor scale at the edge of the inertial subrange and provide a broader inertial subrange.

* Electronic address: hurricane1@llnl.gov

[1] O. Berne, N. Marcelino, and J. Cernicharo, Nature Letters **466**, 947, (2010).

[2] J. W. Miles, J. Fluid Mech. **10**, 496 (1961).

[3] L. P. Bernal and A. Roshko, J. Fluid Mech. **170**, 499 (1986).

[4] D. Papamoschou and A. Roshko, J. Fluid Mech. **197**, 453 (1988).

[5] A. Rikanati, D. Oron, U. Alon, and D. Shvarts, Astrophys. J. **127**, 45 (2000).

[6] O. A. Hurricane, J. F. Hansen, H. F. Robey, B. A. Remington, M. J. Bono, E. C. Harding, R. P. Drake, and C. C. Kuranz, Phys. Plasmas **16** 056305 (2009).

[7] E. C. Harding, J. F. Hansen, O. A. Hurricane, R. P. Drake, H. F. Robey, C. C. Kuranz, B. A. Remington, M. J. Bono, M. J. Grosskopf, and R. S. Gillespie, Phys. Rev. Lett. **103** 045005 (2009).

[8] T. R. Boehly, D. L. Brown, R. S. Craxton, R. L. Keck, J. P. Knauer, J. H. Kelly, T. J. Kessler, S. A. Kumpan, S. J. Loucks, S. A. Letzring, F. J. Marshall, R. L. McCrory, S. F. B. Morse, W. Seka, J. M. Soures, and C. P. Verdon, Opt. Commun. **133**, 495 (1997).

[9] V. A. Smalyuk, J. F. Hansen, O. A. Hurricane, G. Langstaff, D. Martinez, H.-S. Park, K. Raman, B. A. Remington, H. F. Robey, O. Schilling, R. Wallace, Y. Elbaz, A. Shimony, D. Shvarts, C. Di Stefano, R. P. Drake, D. Marion, C. M. Krauland, and C. C. Kuranz, submitted to Phys. Plasmas (2012).

[10] O. A. Hurricane, High Energy Density Phys. **4**, 97 (2008).

[11] O. A. Hurricane, J. F. Hansen, E. C. Harding, V. A. Smalyuk, B. A. Remington, G. Langstaff, H.-S. Park, H. F. Robey, C. C. Kuranz, M. J. Grosskopf, R. S. Gillespie, Astrophys. Space Sci. **336**, 139 (2011).

[12] J. G. Clérouin, M. H. Cherfi, and G. Zérah, Europhys. Lett. **42** , 37 (1998).

[13] A. Rikanati, U. Alon, and D. Shvarts, Phys. Fluids **15**, 3776 (2003).

[14] P.E. Dimotakis, J. Fluid Mech. **409**, 69 (2000).

[15] H. F. Robey, Phys. Plasmas **11**, 4123 (2004).

[16] Y. Zhou, Phys. Plasmas **14**, 082701 (2007).

[17] G. Bazan, *Proceedings from the 2nd International Workshop on Laboratory Astrophysics with Intense Lasers*, (ed. B. A. Remington), UCRL-ID-131978, pp. 42–63, 1998.

[18] R. M. Darlington, T. L. McAbee, and G. Rodrigue, Comp. Phys. Comm. **135**, 3 (2001).

[19] K. S. Raman, O. A. Hurricane, H.-S. Park, B. A. Remington, H. Robey, V. A. Smalyuk, R. P. Drake, and C. C. Kuranz, submitted to Phys. Plasmas (2012).

[20] G. Dimonte and R. Tipton, Phys. Fluids **18**, 085101 (2006).

[21] B.I. Jun, *Private Communication* (2010).

[22] G. L. Brown and A. Roshko, J. Fluid Mech. **64**, 775 (1974).